Microstructural and magneto-transport properties of $Bi_{1.6}Pb_{0.4}Sr_2Ca_{1-x}Gd_xCu_2O_{8+\delta}$ superconducting ceramics

Y. Boudjadja, A. Amira, N. Mahamdioua, A. Saoudel, S. Menassel, A. Varilci, C. Terzioglu, S.P. Altintas

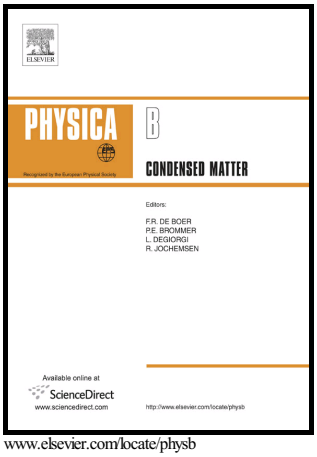

www.elsevier.com/locate/physb

PII: S0921-4526(16)30497-5
DOI: http://dx.doi.org/10.1016/j.physb.2016.10.035
Reference: PHYSB309695

To appear in: *Physica B: Physics of Condensed Matter*

Received date: 25 July 2016
Revised date: 22 October 2016
Accepted date: 24 October 2016

Cite this article as: Y. Boudjadja, A. Amira, N. Mahamdioua, A. Saoudel, S. Menassel, A. Varilci, C. Terzioglu and S.P. Altintas, Microstructural and magneto-transport properties of $Bi_{1.6}Pb_{0.4}Sr_2Ca_{1-x}Gd_xCu_2O_{8+\delta}$ superconductin ceramics, *Physica B: Physics of Condensed Matte* http://dx.doi.org/10.1016/j.physb.2016.10.035

Microstructural and magneto-transport properties of $Bi_{1.6}Pb_{0.4}Sr_2Ca_{1-x}Gd_xCu_2O_{8+\delta}$ superconducting ceramics

Y. Boudjadja [a,*], A. Amira [a], N. Mahamdioua [a], A. Saoudel [a], S. Menassel [b], A.Varilci [c], C. Terzioglu [c], S.P. Altintas [c]

[a] NDT Lab, Faculty of Science and Technology, Jijel University, Jijel 18000, Algeria

[b] MSAR Unit, Physics Department, Constantine 1 University, Constantine 25017. Algeria

[c] Department of Physics, Faculty of Arts and Sciences, AIB University, Bolu 14280, Turkey

[*]Corresponding author. Tel.: +213 670 09 13 83; Fax: +213 34 50 11 89.
yazid.bouj@Gmail.com

Abstract

This study aims to investigate the effect of Gd doping on the phase formation, microstructure, transport and magnetic properties of the Bi(Pb)-2212 system. A series of superconducting bulks with a nominal composition of $Bi_{1.6}Pb_{0.4}Sr_2Ca_{1-x}Gd_xCu_2O_{8+\delta}$ with x = 0, 0.05, 0.10 and 0.15 are synthesized by the solid state synthesis route. The formed samples are characterized by means of X-ray diffraction analysis (XRD), scanning electron microscopy (SEM), energy dispersive X-ray spectrometer (EDS), electrical transport and magnetic measurements. The experiment results reveal that all the samples doped are composed of Bi-2212 phase and traces of Bi-2201 secondary phase when compared to the undoped sample. The refinement of cell parameters shows that the doping reduces the cell volume of the samples. The texture degree decreases with doping while the degree of orthorhombicity increases. Quantitative EDS analysis confirms that Gd atoms are successfully introduced into crystalline structure. The SEM micrographs show randomly distributed grains with a flake-like shape. The highest value of onset critical transition temperatures is obtained for x = 0.10 and is about 90.22 K, which correlates well with the observed slope of resistivity and the hole concentration of the CuO_2 layers. Magnetic hysteresis loops suggest that the diamagnetism, remanant magnetization and lower critical field are better for x = 0.10. Based on the enhancements of both grain boundary weak-links and flux pinning centers, improvement of the critical current densities and flux pinning density is obtained with this kind of doping.

Keywords

Bi-2212; HTSC; critical current density; hysteresis loops; flux pinning

1. Introduction

In more than three decades elapsed from the discovery of High-T_c cuprate superconductors (*HTSC*) by Bednorz and Müller [1], practical superconducting wires made of these materials are now being manufactured, and trials of electrical and industrial applications including a train supported by magnetic levitation, a transmission line, a ship's engine, and many others are being implemented [2-6]. The description of the physical properties of *HTSC* has turned out to represent a big challenge to solid-state physics theory. The difficulty of this problem is due to the complicated properties, including crystalline structures of materials displaying high superconducting critical transition temperature (T_c), the presence of a strong anisotropy, high electronic correlations and electron–phonon interactions. It is well known that there are three different phases in the Bi-based superconducting oxides ($Bi_2Sr_2Ca_{n-1}Cu_nO_{2n+4+\delta}$, n =1, 2, 3). These phases are Bi-2201, Bi-2212 and Bi-2223 having T_c values around 20 K, 80 K, and 110 K, respectively [**7**]. Bi-2212 phase is the most important of these series because of its high stability and facility of preparation with very high proportion. Also, its oxygen stoichiometry is relatively invariant with respect to cationic doping when the samples are prepared in identical conditions [8,9]. The problem of weak links is then less pronounced when compared to Bi-2223 phase having the highest T_c. An understanding of the electrical and magnetic properties of the *HTSC* must start out from an analysis of their electronic structure, chemical composition, valences, oxygen content as well as preparation conditions. The topic of inhomogeneities has always been present in *HTSC* systems. Initially, it is simply due to (i) the oxygen non-stoichiometry necessary to dope the materials, and to (ii) the difficulty in producing homogeneous samples even on a several-nanometer scale. The Bi-based superconductors have layered perovskite-like crystal structures which consist of conducting CuO_2 planes separated by donor metal oxide layers. Doping the CuO_2 layers with holes or the creation of oxygen vacancies in charge reservoirs outside the conducting planes causes the appearance of new electronic ordered states. We noticed that, based on the layered structure of Bi-2212 system, Ca layer is located between two CuO_2 layers. Also, the unit cell contains two semiconducting BiO and two insulating SrO layers. The microstructure of Bi-based oxide superconductors consists of plate-like grains with the *a–b* plane along the flat surface of the platelets. If the grains are aligned by stacking the platelets like a structure of bricks [10], a high critical current density (J_c) can be achieved in the *a–b* plane. The effect of substitution of cations on the superconducting properties of Bi-2212 system has been a subject of great interest for both technologists and theoreticians. This is because doping is an effective method for improving the structural, transport, superconducting and flux pinning properties of Bi-based superconductors making them suitable for the application at higher temperatures and

magnetic fields. The doping by lead of Bi-2212 phase is found to improve the highest onset critical transition temperature ($T_{c,on}$), flux pinning properties (irreversibility line and J_c in applied fields) and reduces structural modulation [11-13]. The rare earth elements have an incomplete inner shell, different magnetic moments and different ionic radii. Therefore, they have great importance as a substitute for studying the physical properties of *HTSC*. The magnetic field dependent transport properties, flux pinning mechanism, grain connection phenomena, thermal properties and crystallization kinetics of *HTSC* have been investigated by many groups [14-16]. Enormous works have focused on the effect of high doping by different elements of the lanthanides series (La, Ce, Pr, Nd, Sm, Eu, Dy, Ho …) at Ca or Sr sites of Bi-2212 phase [17-19]. In general, most of these studies reported that the superconducting properties are better when the doping is realized between the CuO_2 planes at the Ca site.

As a contribution to this field of research, this paper reports on synthesis and characterization of bulk polycrystalline Gd doped (Bi,Pb)-2212 phase at Ca site. The study is carried out by analyzing magnetization and resistivity results.

2. Experimental details

Various methods like de-carbonation, co-precipitation, melt process, spray pyrolysis and sol-gel synthesis routes are adopted today for the preparation of superconductors. Because of its reproducibility and simplicity, the solid state reaction method is adopted in this work. The nominal composition of the prepared samples is $Bi_{1.6}Pb_{0.4}Sr_2Ca_{1\_x}Gd_xCu_2O_{8+\delta}$ with x = 0, 0.05, 0.10 and 0.15. They will be labelled CG00, CG05, CG10 and CG15, respectively. The starting chemical powders are corresponding stoichiometric quantities of high-purity Bi_2O_3, PbO, $SrCO_3$, $CaCO_3$, CuO and Gd_2O_3. The mixture powders are hand milled in an agate mortar, calcined in air at 800 °C during 12 h. The resultant materials are grinded and pressed into pellets under a pressure of 20 kN using a cylindrical die. They are then submitted to two successive cycles of sintering in air at 825 °C /24 h and 850 °C /24 h, with an intermediate grindings and pressings. X-ray powder diffraction (XRD) is performed at room temperature on a Rigaku D/Max-IIIC diffractometer with CuKα radiation with an angle step of 0.02°. Phase identification is performed using the ICDD-PDF2 database. The refinement of cell parameters is realized by use of Janna2006 software. Microstructural examinations and surface morphology are done on a JEOL JSM-6390LV scanning electron microscope (SEM) equipped with an Oxford energy dispersive spectrometer (EDS). The temperature dependence of resistivity is performed on a closed cycle helium refrigerator (Cryodine CTI-Cryogenics)

by use of a standard four probe technique. The contacts are made by the silver paint to rescue the extra resistivity. The magnetisation measurements $M(H)$ are registred in the Zero Field Cooled (ZFC) mode at 5K on a Vibrating Sample Magnetometer (PPMS-9T).

3. Results and Discussion

Fig. 1 shows the X-ray diffraction patterns of $Bi_{1.6}Pb_{0.4}Sr_2Ca_{1-x}Gd_xCu_2O_{8+\delta}$ polycrystalline samples. The corresponding (*hkl*) Miller indices of the observed lines are also shown on the diagrams. As can be seen, all of samples consist of dominant Bi-2212 [JCPDS-ICDD 41-0317 file]. The Bi-2201 phase is the only minor detected one [JCPDS-ICDD 46-0392 file]. Its characteristic peaks are marked by ♦ symbol. This result also reflects that the phase stability limit of Bi-2212 phase can be extended to smaller rare earth ions like Gd. However, XRD patterns show that the peaks intensities of Bi-2201 secondary phase increase slightly with doping. To reduce the degradation of Bi-2212 to Bi-2201 ratio, it is important then to perform a doping by low content of gadolinium. The oxygen stoichiometry and weak coupling between BiO–BiO layers plays a crucial role in the production of non-superconducting secondary phases [20]. The samples studied do not exhibit any different phases including Gd atoms, indicating its complete solubility in the Bi-2212 superconducting crystal structure. These results are verified through Reitveld refinement by using Jana2006 program [21]. Thus, these compounds crystallize in the orthorhombic structure with *Bbmb* space group [22]. The superposition of the observed and calculated diffraction patterns of each sample is given in the insets of Fig. 1. The obtained cell parameters as well as the refinement factors (R_p, R_{wp}) and the goodness of fit (GOF) are listed in Table 1, which are close to those obtained by many groups [22-25]. The variation of *a* and *b* parameters seems to be independent of gadolinium doping while *c* decreases monotonously as well as the cell volume. The behavior of *a* and *b* lattice parameters is generally associated with the increase in the Cu–O bond length which controls the dimension of the basal plane [23]. The reduction of volume indicates that the Gd ions are readily incorporated into the structure and could be associated to the difference between ionic radius of Gd^{3+} (0.93 Å) and that of the substituted Ca^{2+} (0.99 Å) one [26]. The intensities of the (*0 0 l*) diffraction lines are found to be important which indicates that the grains are preferentially oriented along the *c*-axis. The degree of texture is estimated by:

$$F_{00l} = \sum I_{00l} / (\sum I_{2212} + \sum I_{sp}) \times 100\% \qquad (1)$$

Where I_{00l} represents the intensity of (*0 0 l*) diffraction peaks of Bi-2212, I_{2212} is the total diffraction intensity of Bi-2212, and I_{sp} is the total diffraction intensity of the secondary phase (Bi-2201). Textural structure is a crucial factor for the intergrain in superconductors. The obtained degrees of texture and orthorhombicity (*b* - *a*)/*b* are listed in Table 1. F_{00l} decreases with Gd doping from 23.79 % (CG00) to 14.48 % (CG15) while the degree of orthorhombicity reaches its highest value for CG10 sample corresponding to *x=0.1*.

In order to analyze the mean values of the elemental composition of our bulk samples, energy dispersive X-ray spectroscopy (EDS) is used. The EDS spectrums illustrated in Fig. 2 show the elemental distribution in the samples. The atomic contents of elements for each sample are also given in the insets of Fig. 2. The results demonstrate that there is no undesirable element in all samples. Upon increasing Gd content, it is found that the Ca content decrease which confirms that the doping element is effectively incorporated into crystalline structure of the samples. The peak intensities of the elements such as Bi, Pb, Sr and Cu are not affected and its atomic concentrations are nearly the same for all samples. The values of oxygen content are gradually increased which leads to an increase in the carrier concentration. When trivalent Gd ion substitutes for divalent Ca one, the excess of positive charge is compensated by incorporation of extra oxygen atoms in the BiO planes [27,28]. The microstructure of samples plays an important role to determine the transport properties. The micrographs of the surface of the pellets are obtained using scanning electron microscopy (SEM) as shown in Fig. 3. They are taken in the secondary electron image at 3000× magnification. The shape of the grains is no more affected by Gd doping suggesting that the doping element my not change the melting point of Bi(Pb)-2212 phase. This result may be due to the weak Vander Waal's forces between oxide layers in which Gd can be easily introduced during treatment process. Furthermore, the grain morphology illustrates clear a flake-like shape of the grains with layered growth and some pores. In the doped samples, one can observe that the grain connectivity is slightly worsened. This is related to the stable behaviour of Gd ions in the crystal structure of Bi(Pb)-2212 system where it is more active than the Ca ion due to its small ionic radius. As it can be seen, the CG10 sample has smaller and more homogenous grain size and relatively low number of boundaries compared to other samples, indicating rich formation of the superconducting phase.

The dc electrical resistivity versus temperature curves are given in Fig. 4. Some superconducting parameters are extracted from these curves and listed in Table 2. It is found that all the samples reveal a metallic character above the onset critical transition temperature $T_{c,on}$ from which they exhibit a superconducting behaviour. As a general way, each sample

shows a sharp transition into the superconducting state. However, the values of superconducting critical temperatures are very sensitive to gadolinium content. The highest value of $T_{c,on}$ is obtained for CG10 sample and is about 90.22 K. Induction of mobile carriers, overall oxygen content and disorder in the CuO_2 planes are possible mechanisms responsible of the variation of $T_{c,on}$ [29]. It is well known that the offset critical transition temperature $T_{c,off}$ generally gives information about weak links of the superconductor grains and grain boundaries, while $T_{c,on}$ can reveal the superconducting phases occurred in the grain structure. It is clearly evident that the $T_{c,off}$ values are nearly the same for CG00, CG05 and CG10 samples suggesting that doping by Gd do not affect the intergranular weak links contrary to the grain structure. It is obvious that, all samples show almost a very narrow width of transition temperature (ΔT_c) illustrating a single superconducting transition. Contrary to this, large transition widths can be associated with the high disorientation angle which decreases the intergranular coupling [30]. The normal state resistivity of the granular superconducting sample is given by:

$$\rho(T) = \alpha + \beta T \qquad (2)$$

where α presents the residual resistivity of the materials. It is related to the defect interfaces such as grain boundaries, stacking faults, voids, planar and micro-defects of the materials [31-33]. As shown in Table 2, the value of α decreases until reaching a minimum at $x = 0.10$. This decrease of α with Gd doping attests of a increase of the hole concentration or of an extension of the relaxation time of charge carriers due to a little number of defects created by a systematic distribution of the doping element. It is also visible from resistivity curves in the normal state that there are also small curvatures. This phenomenon may result from thermodynamic fluctuations or an opening of pseudogap. The slope of resistivity curve β may be considered as a parameter that depends on intrinsic electronic interactions [34]. The maximum of β is also seen for CG10 sample which correlates well with the obtained value of $T_{c,on}$. The enhancement of superconducting properties in BSCCO system is attributed to the optimization of hole concentration in the CuO_2 layers. The hole concentrations P per Cu ion are calculated by using the generic parabolic law:

$$T_{c,on}/T_{c,max} = 1 - a\,(P - P_0)^2 \qquad (3)$$

where $T_{c,max}$ = 95 K for Bi-2212 [35], a= 82.6 determines the doping range for occurring superconductivity and P_0= 0.16 corresponds to the optimal hole density (when $T_{c,on} = T_{c,max}$). The variation of the hole-carrier concentration versus Gd content is also depicted in the insets

of Fig. 4. The optimal doping level suggests the occurrence of an electronic phase transition separating the underdoped and overdoped regimes in the parabolic behavior. Therefore, it can be indicated that the doping changes the samples behavior from overdoped region to optimally doped one. One can see from Table 2, the obtained minimum hole number of 0.184 for CG10 sample suggests that is closer to the optimally dopesd region. The substitution of trivalent Gd^{3+} for divalent Ca^{2+} leads then to a reduction of the number of effective holes, and the usually increasing of the oxygen content is insufficient to compensate for the charge change. As a consequence, a decrease of the number of holes in the CuO_2 planes is obtained. The $T_{c,on}$ of all samples is also found to correlate well with the hole concentration of the CuO_2 layers.

Fig. 5 depicts magnetization curves for studied samples measured at temperature 5 K under magnetic field up to 9 T. All the hysteresis loops are measured in the zero-field cooled (*ZFC*) mode. Magnetic hysteresis cycles in *HTSC* allow us to reveal much important information [36]. The *M–H* curves exhibit a characteristic behaviour and reveal that Gd doping has an important influence on the hysteresis width which corresponds to the difference between the upper and the lower braches of the loop. All of the curves clearly show an exponential decay of the width ΔM of the hysteresis loop when the magnetic field is increased. At very low fields, the *M-H* loop is a reversible straight line with a slope of magnitude equal to the superconducting volume fraction of the samples. The ΔM of the bulk samples shows its higher value for $x = 0.10$. ΔM increases because of the development of inter-granular currents when new pinning centers of fluxons are created. Furthermore, the remanant magnetization M_R values are identified when the applied field is removed at zero (see Table 3). These results also suggest that the diamagnetism and pinning strength of the CG10 sample are better than the others ones, resulting in reduction of grain boundaries. It is well established that the pinning strength in the superconductor materials is directly proportional to M_R. The deviation point of the M (H) virgin curve from linearity (Meissner line) gives the value of the first penetration field H_{c1}^{*}, where the vortex starts entering into the sample. All of the curves clearly show the common linear dependence of the magnetic moment on the field associated with the Meissner effect. The value of lower critical field H_{c1} can be derived as given by Brandt [37]:

$$H_{c1}^{*} = H_{c1} / \tanh (0.36b/a)^{1/2} \qquad (4)$$

where *a* and *b* are the width and thickness of the sample, respectively. The field dependence of initial magnetization curves is given in the inset of Fig. 5. The H_{c1} is directly related to the free energy of a flux line and contains information on essential mixed state parameters while H_{c1}* is a decreasing function of temperature and degree of sample shape deformation [38,39]. The highest value of H_{c1} and the maximum of the slope of the curve are always seen for CG10 sample, confirming then the higher superconducting volume fraction for this level of doping. According to the Bean's critical state model for the field independent critical current density, the J_c is determined by [40]:

$$J_c = 30\,(M^+ - M^-)/a(1 - a/3b) \qquad (5)$$

where M^+ and M^- are the values of magnetization when sweeping fields up and down, respectively, *a* and *b* are the dimensions of the cross-section of the bars ($a < b$). As shown in Fig. 6, a nearly exponential decrease of J_c with magnetic field is obtained for each sample. A large hysteresis curves and high magnetization values lead to highest J_c values (see Table 3). An evident increase in J_c of almost 42% in magnitude is obtained for $x = 0.10$ when compared to the Gd free sample. This trend is related to the reduction of the intrinsic anisotropy of CG10 sample and to the fact that the doping can furnish new favourable pinning centres which are effective at higher fields [41]. The reduction of the J_c value for CG15 sample is related to the retrogression of the vortices in the crystal system due to the grain boundary resistivity and weak links [42]. Inset of Fig. 6 shows the flux pinning density given by $F_p = J_c \times B$ for the samples at 5K [43]. The F_p in *SHTC* is influenced by size and shape of pinning sites, microstructure, flux lattice rigidity and thermodynamic properties of the material [44,45]. As given in table 3, the results show an improvement in flux pinning with Gd doping at the same value of *x= 0.10*. The gadolinium elements disperse in the superconducting matrix and can act as effective flux pinning centers. Also, the bridging of two Cu-O_2 planes by Ca^{2+} is accompanied by the creation of flux pinning centers, as structural defects are created when smaller ion Gd^{3+} replaces bigger Ca^{2+} one in the unit cell.

4. Conclusion

In summary, synthesis and characterization of $Bi_{1.6}Pb_{0.4}Sr_2Ca_{1-x}Gd_xCu_2O_{8+\delta}$ superconductors have been carried in the range $0 \le x \le 1.5$. Doping by low amounts of Gd^{3+} ions is observed to be effective on phase formation, grain connectivity, hole carrier concentration, superconducting behaviour, diamagnetism and flux pinning. The results demonstrated that the

enhancement of coupling between the CuO_2 planes, the critical current densities and flux pinning density is obtained for the sample with $x = 0.10$.

References

[1] J.G. Bednorz, K.A. Müller, Possible high T_c superconductivity in the Ba−La−Cu−O system, Z. Phys. B 64 (1986) 189-193.

[2] T. Masuda, T. Kato, H. Yumura, M. Watanabe, Y. Ashibe, K. Ohkura, C. Suzawa, M. Hirose, S. Isojima, K. Matsuo, S. Honjo, T. Mimura, T. Kuramochi, Y. Takahashi, H. Suzuki, T. Okamoto, Verification tests of a 66 kV HTSC cable system for practical use (first cooling tests), Physica C 378 (2002) 1174-1180.

[3] T. Kurusu, M. Ono, S. Hanai, M. Kyoto, H. Takigami, H. Takano, K. Watanabe, S. Awaji, K. Koyama, G. Nishijima, K. Togano, A cryocooler-cooled 19 T superconducting magnet with 52 mm room temperature bore, IEEE Trans. Appl. Supercond. 14 (2004) 393-396.

[4] M.C. Cheng, B.P. Yan, K.H. Lee, Q.Y. Ma, E.S. Yang, A high temperature superconductor tape RF receiver coil for a low field magnetic resonance imaging system, Supercond. Sci. Technol. 18 (2005) 1100-1105.

[5] K. Suzuki1, J. Baba, T. Nitta, Conceptual design of an SFCL by use of BSCCO wire, J. Phys. Conf. Ser. 97 (2008) 012293-012296.

[6] B.A. Albiss, Thick films of superconducting YBCO as magnetic sensors, Supercond. Sci. Technol. 18 (2005) 1222-1226.

[7] H. Maeda, Y. Tanaka, M. Fukutomi, T. Asano, A New High-T_c Oxide Superconductor without a Rare Earth Element, Jpn. J. Appl. Phys. 27 (1988) L209-L210.

[8] J.M. Tarascon, P. Barboux, G.W. Hull, R. Ramesh, L.H. Greene, M. Gariod, M.S. Hedge, W.R. Mckinnon, Bismuth cuprate high-Tc superconductors using cationic substitution, Phys. Rev. B 38 (1989) 43164326.

[9] K. Koyama, S. Kanno, S. Noyuchi, Electrical, Magnetic and Superconducting Properties of the Quenched $Bi_2Sr_2Ca_{1-x}Nd_xCu_2O_{8+\delta}$ System, Jpn. J. Appl. Phys. 29 (1990) L53-L56.

[10] S. Martin, A.T. Fiory, R.M. Fleming, G.P. Espinosa, A.S. Cooper, Anisotropic critical current density in superconducting $Bi_2Sr_2CaCu_2O_8$ crystals, Appl. Phys. Lett. 54 (1989) 72-74.

[11] N. Musolino, S. Bals, G. vanTendeloo, N. Clayton, E. Walker, R. Flükiger, Investigation of (Bi,Pb)2212 crystals: observation of modulation-free phase, Physica C 401 (2004) 270-272.

[12] I. Chong, Z. Hiroi, M. Izumi, J. Shimoyama, Y. Nakayama, K. Kishio, T. Terashima, Y. Bando, M. Takano, High critical current density in the heavily Pb-doped $Bi_2Sr_2CaCu_2O_{8+\delta}$ generation of novel pinning centers, Science 276 (1997) 770-773.

[13] H.W. Zandbergen, W.A. Groen, A. Smit, G. van Tendeloo, Structure and properties of (Bi, Pb)$_2$Sr$_2$(Ca, Y)$Cu_2O_{8+\delta}$, Physica C 168 (1990) 426-449.

[14] N. Ghazanfari, A. Kilic, A. Gencer, H. Ozkan, Effects of Nb_2O_5 addition on superconducting properties of BSCCO, Solid State Commun. 11 (2007) 210-214.

[15] M.I. Adam, Effect of magnetic element ions on collective pinning behaviour in Bi-2223 quadrilateral bars, Physica C 463 (2007) 439-444.

[16] M.A. Aksan, M.E. Yakinci, Synthesis and characterization of Er-substituted Bi-2223 H-T_c glass–ceramic superconductors, J. Alloys Compd. 385 (2004) 33-43.

[17] A. Biju, K. Vinod, R.P. Aloysius, U. Syamaprasad, Improved superconducting properties by La addition in (Bi,Pb)-2212 bulk superconductor, J. Alloys Compd. 431 (2007) 49-55.

[18] A. Sedky, On the influence of rare-earth substitution for Ca in Bi(Pb):2212 superconducting system, Physica C 468 (2008) 1041-1046.

[19] S. Vinu, P.M. Sarun, R. Shabna, A. Biju, U. Syamaprasad, Microstructure and transport properties of $Bi_{1.6}Pb_{0.5}Sr_{2-x}Lu_xCa_{1.1}Cu_{2.1}O_{8+\delta}$ superconductor, Mater. Chem. Phys. 119 *(*2010) 135-139.

[20] P. Majewski, Phase diagram studies in the system Bi-Pb-Sr-Ca-Cu-O-Ag, Supercond. Sci. Technol. 10 (1997) 453-468.

[21] V. Petricek, M. Dusek, L. Palatinus, The Crystallographic Computing, Institute of Physics, Praha, Czech Republic, 2006 (JANA2006).

[22] A. Amira, Y. Boudjadja, A. Saoudel, A. Varilci, M. Akdogan, C. Terzioglu, M.F. Mosbah, Effect of doping by low content of yttrium at Ca and Sr sites of Bi(Pb)-2212 superconducting ceramics, Physica B 406 (2011) 1022-1027.

[23] R. Shabna, P.M. Sarun, S. Vinu, U. Syamaprasad, Superconductor–metal–insulator crossover in $Bi_{1.7}Pb_{0.4}Sr_{2-x}Ce_xCa_{1.1}Cu_{2.1}O_{8+\delta}$ ($0.2 \le x \le 0.6$) sintered between 845 °C $\le T_s \le$ 865 °C, Mater. Sci. Eng. B 172 (2010) 196-200.

[24] A. Biju, P.M. Sarun, R.P. Aloysius, U. Syamaprasad, Comparison of superconducting properties of Ce added (Bi, Pb)-2212 with other rare earth additions, J. Alloys Compd. 433 (2007) 68-72.

[25] Y. Boudjadja, A. Amira, A. Saoudel, A. Varilci, S.P. Altintas, C. Terzioglu, Structural and electrical properties of cerium doped Bi(Pb)-2212 phases, Physica B 443 (2014) 130-135.

[26] R.D. Shannon, Acta Crystallogr. A 32 (1976) 751-767.

[27] N. Fukushima, H. Nui. S. Nakamura, S.Takeno. M. Hayashi, K. Ando, Structural modulation and superconducting properties in $Bi_{2-x}Pb_xSr_2CaCu_2O_{8+d}$ and $Bi_{2-y}Pb_ySr_2YCu_2O_{8+d}$, Physica C 159 (1989) 777-783.

[28] A.Q. Pham, M. Hervieu, A. Maignan, C. Michel, J. Provost, B. Raveau, Relationships between composition, oxygen non-stoichiometry, structure modulation and superconductivity in the“2212”bismuth cuprates, Physica C 194 (1992) 243-252.

[29] A.R. Moodenbaugh, D.A. Fischer, U.Y.L. Wang, Y. Fukumoto, Superconductivity, oxygen content, and hole state density in $Bi_2Sr_{1.75}Ca_{1.25}Cu_2O_{8.18+y}$ ($-0.09 < y \le 0$) and $Bi_{1.6}Pb_{0.4}Sr_{1.9}Ca_2Cu_3O_z$, Physica C 268 (1996) 107-114.

[30] Ph. Vanderdemden, A.D. Bradley, R.A. Doyle, W. Lo, D.M. Astill, D.A. Cardwell, A.M. Campbell, Superconducting properties of natural and artificial grain boundaries in bulk melt-textured YBCO, Physica C 302 (1998) 257-270.

[31] C. Autret-Lambert, B. Pignon, M. Gervais, I. Monot-Laffez, A. Ruyter, L. Ammor,F. Gervais, J.M. Bassat, R. Decourt, Microstructural and transport properties in substituted $Bi_2Sr_2CaCu_2O_{8+\delta}$-modulated compounds, J. Solid State Chem. 179 (2006) 1698-1706.

[32] H. Hilgenkamp, J. Mannhart, Grain boundaries in high-Tc superconductors, Rev. Mod. Phys. 74 (2002) 485-549.

[33] M.L Li, Y. Zhang, Y. Li, Y. Qi, Granular superconductivity in polycrystalline $Bi_2Sr_2CaCu_2O_{8+\delta}$ by homovalent La, J. Non-Cryst. Solids 356 (2010) 2831-2835.

[34] B. Pignon, C. Autret-Lambert, A. Ruyter, R. Decourt, J.M. Bassat, I. Monot-Laffez, L. Ammor, Study of the yttrium and zinc substitutions effects in $Bi_2Sr_2CaCu_2O_{8+\delta}$ compounds by transport measurements, Physica C 468 (2008) 865-871.

[35] M.R. Presland, J.L. Tallon, R.G. Buckley, R.S. Liu, N.E. Flower, General trends in oxygen stoichiometry effects on T_c in Bi and Tl superconductors, Physica C 176 (1991) 95-105.

[36] B.A. Albiss, I.M. Obaidat, M. Gharaibeh, H. Ghamlouche, S.M. Obeidat, Impact of addition of magnetic nanoparticles on vortex pinning and microstructure properties of Bi–Sr–Ca–Cu–O superconductor, Solid State Commun. 150 (2010) 1542-1547.

[37] E.H. Brandt, Irreversible magnetization of pin-free type-II superconductors, *Phys. Rev.* B 60 (1999)11939-11942.

[38] C. Böhmer, G. Brandstätter, H.W. Weber, The lower critical field of High-Temperature Superconductors, Supercond. Sci. Technol. 10 (1997) A1-A10.

[39] Y. Enomoto, K. Okada, Simulation study on the first penetration field in type-II superconductors, J. Phys. Cond. Matter 9 (1997) 10203-10209.

[40] C.P. Bean, Magnetization of High-Field Superconductors, Rev. Mod. Phys. 36 (1964) 31-39.

[41] Y. Li, S. Kaviraj, A. Berenov, G.K. Perkins, J. Driscoll, A.D. Caplin, G.H. Cao, Q.Z. Ma, B. Wang, L. Wei and Z.X. Zhao, Enhancement of critical current density of (Pb,Sn)-doped Bi-2212 superconductors at high temperature, Physica C 335 (2001) 51-58.

[42] M. Dogruer, Y. Zalaoglu, G. Yildirim, A. Varilci, C. Terzioglu, Effect of diffusion-annealing time ($0.5\ h \leq t \leq 2\ h$) on the mechanical and superconducting properties of Cu-diffused bulk MgB_2 superconductors by use of experimental and different theoretical models, J. Mater. Sci. Mater. Electron. 24 (2013) 2019-2026.

[43] M.R. Koblischka, M. Murakami, Pinning mechanisms in bulk high-*Tc* superconductors, Supercond. Sci. Technol. 13 (2000) 738-744.

[44] D. Dew-Hughes, Flux pinning mechanisms in type II superconductors, Philosophical Magazine 30 (1974) 293-305.

[45] K. Okamura, M. Kiuchi, E.S. Otabe, T. Yasuda, T. Matsushita, S. Okayasu, The pinning property of Bi-2212 single crystals with columnar defects, Supercond. Sci. Technol. 17 (2004) S20-S24.

Fig. 1. XRD patterns of $Bi_{1.6}Pb_{0.4}Sr_2Ca_{1-x}Gd_xCu_2O_{8+\delta}$ samples. Insets: superposition of experimental and calculated patterns.

Fig. 2. EDS spectrums of $Bi_{1.6}Pb_{0.4}Sr_2Ca_{1-x}Gd_xCu_2O_{8+\delta}$ bulks. Insets: atomic contents of elements of each sample.

Fig. 3. SEM micrographs of resistivity for $Bi_{1.6}Pb_{0.4}Sr_2Ca_{1-x}Gd_xCu_2O_{8+\delta}$ samples.

Fig. 4. Temperature dependence of resistivity for $Bi_{1.6}Pb_{0.4}Sr_2Ca_{1-x}Gd_xCu_2O_{8+\delta}$ samples. Insets: $T_{c,on}$ and Hole-carrier concentration vs Gadolinium content.

Fig. 5. Magnetic hysteresis loops measured at 5 K for $Bi_{1.6}Pb_{0.4}Sr_2Ca_{1-x}Gd_xCu_2O_{8+\delta}$ samples. The inset displays the field dependence of initial magnetization curves.

Fig. 6. Critical current densities of $Bi_{1.6}Pb_{0.4}Sr_2Ca_{1-x}Gd_xCu_2O_{8+\delta}$ samples at 5K as a function of applied field. Inset: variation of pinning force versus magnetic field.

Table 1 Cell parameters (*a*,*b*,*c*), cell volume *V*, agreement factors (R_p,R_{wp}), goodness of fit (GOF), degree of orthorhombicity and texture degree of of $Bi_{1.6}Pb_{0.4}Sr_2Ca_{1-x}Gd_xCu_2O_{8+\delta}$ samples.

	***a* (Å)**	***b* (Å)**	***c* (Å)**	***V* (Å^3)**	***(Rp,Rwp) %***	***GOF***	***(b-a)/b* (%)**	**F_{00l} (%)**
CG00	5.394 (2)	5.398 (2)	30.759 (3)	895.9 (2)	(10.55,14.56)	2.57	0.0741	23.79
CG05	5.396 (1)	5.404 (1)	30.701 (2)	895.5 (1)	(9.62,13.55)	2.46	0.140	21.92
CG10	5.385 (1)	5.423 (9)	30.676 (4)	894.4 (3)	(11.27,15.54)	2.74	0.700	15.77
CG15	5.387 (3)	5.391 (3)	30.621 (9)	889.4 (6)	(11.67,16.41)	2.79	0.0742	14.48

Table 2 Onset ($T_{c,on}$) and offset ($T_{c,off}$) critical transition temperatures, transition width (ΔT_c), residual resistivity (α), slope (β) of resistivity and hole-carrier concentration (P) of $Bi_{1.6}Pb_{0.4}Sr_2Ca_{1-x}Gd_xCu_2O_{8+\delta}$ samples.

Samples	$T_{c,on}$	$T_{c,off}$	ΔT_c	α	β	P	
	(K)	**(Ω.Cm)**	**(Ω.cm.K^{-1})**	***([hole-carrier]/Cu)***		**(K)**	**(K)**
CG00	78,89	68,24	10,65	$2{,}10.10^{-3}$	$6{,}95.10^{-6}$	0.205	
CG05	86,11	68,97	17,14	$1{,}83.10^{-3}$	$7{,}04.10^{-6}$	0.193	
CG10	90,22	70,53	19,69	$1{,}64\ .10^{-3}$	$8{,}91.10^{-6}$	0.184	
CG15	78,06	58,26	19,80	$1{,}92\ .10^{-3}$	$8{,}52.10^{-6}$	0.206	

Table 3 Critical current density (J_c), force pinning maximal ($F_{p\text{-}max}$), remnant magnetization (M_R) and lower critical field (H_{c1}) of $Bi_{1.6}Pb_{0.4}Sr_2Ca_{1-x}Gd_xCu_2O_{8+\delta}$ samples.

	J_c	$F_{p\text{-}max}$	M_R	H_{c1}
	(A/cm^2) at 5K, 0 T	**(N/m^3)**	**(emu/cm^3)**	**(mT)**
CG00	27.01 10^3	26.65 10^6	16.59	0.93
CG05	34.32 10^3	41.35 10^6	26.52	1.08
CG10	47.17 10^3	64.70 10^6	42.96	1.16
CG15	17.33 10^3	22.06 10^6	11.25	0.75

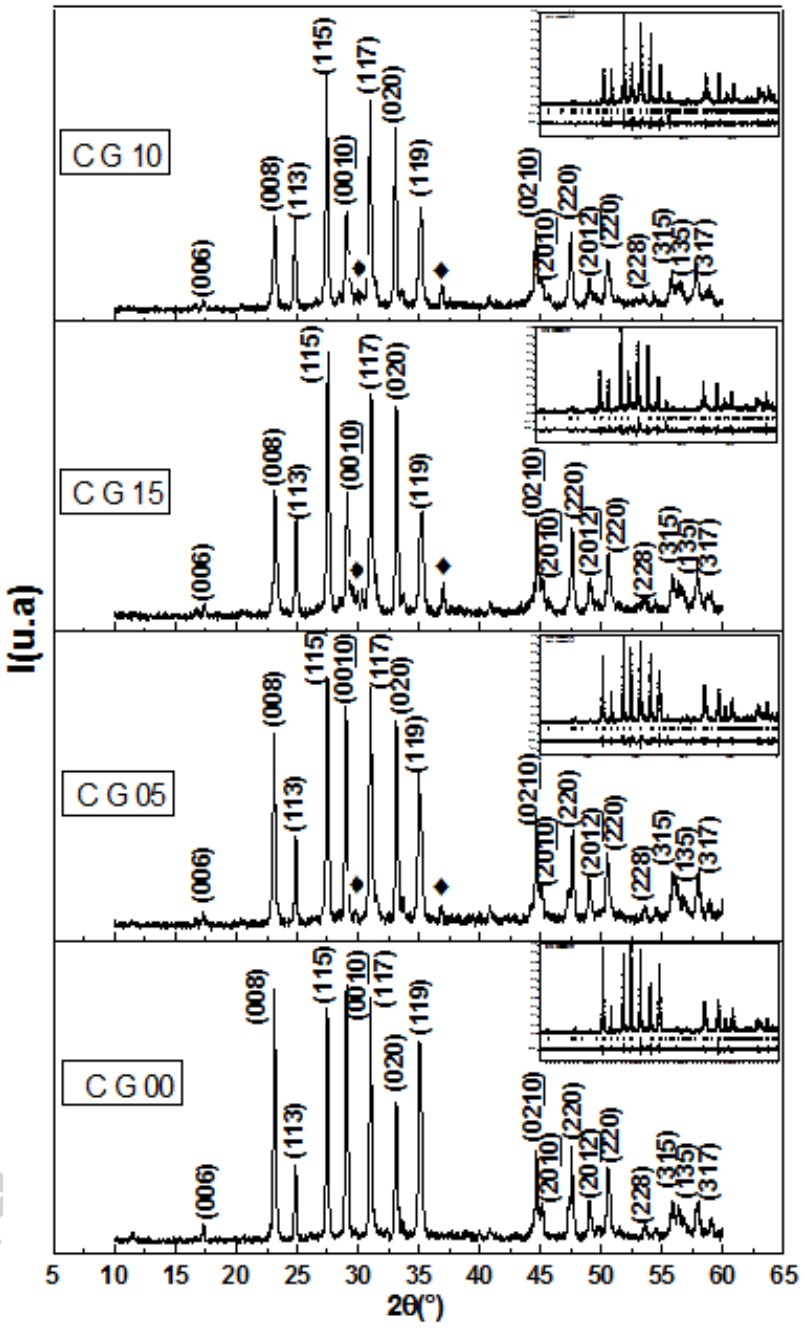

Fig. 1. XRD patterns of $Bi_{1.6}Pb_{0.4}Sr_2Ca_{1-x}Gd_xCu_2O_{8+\delta}$ samples. Insets: superposition of experimental and calculated patterns.

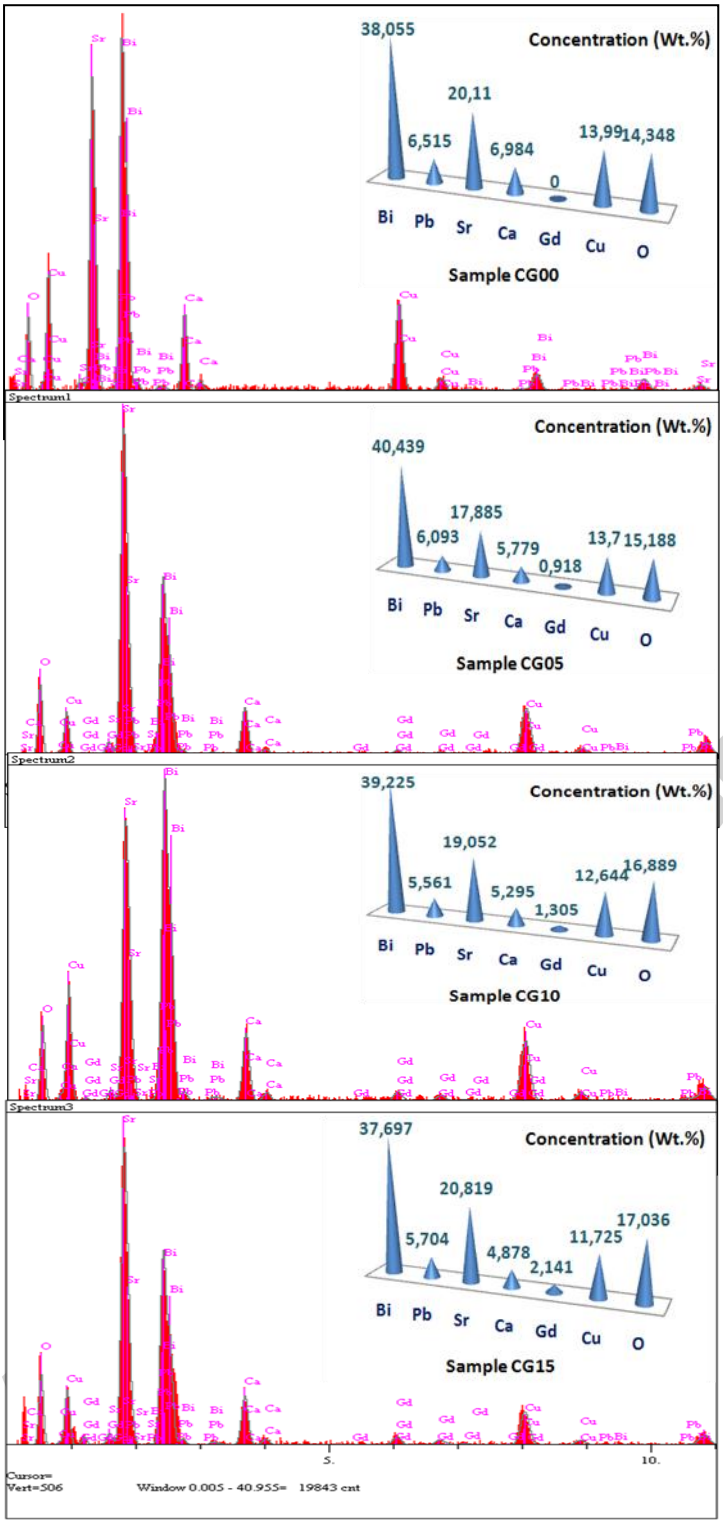

Fig. 2. EDS spectrums of $Bi_{1.6}Pb_{0.4}Sr_2Ca_{1-x}Gd_xCu_2O_{8+\delta}$ bulks. Insets: atomic contents of elements of each sample.

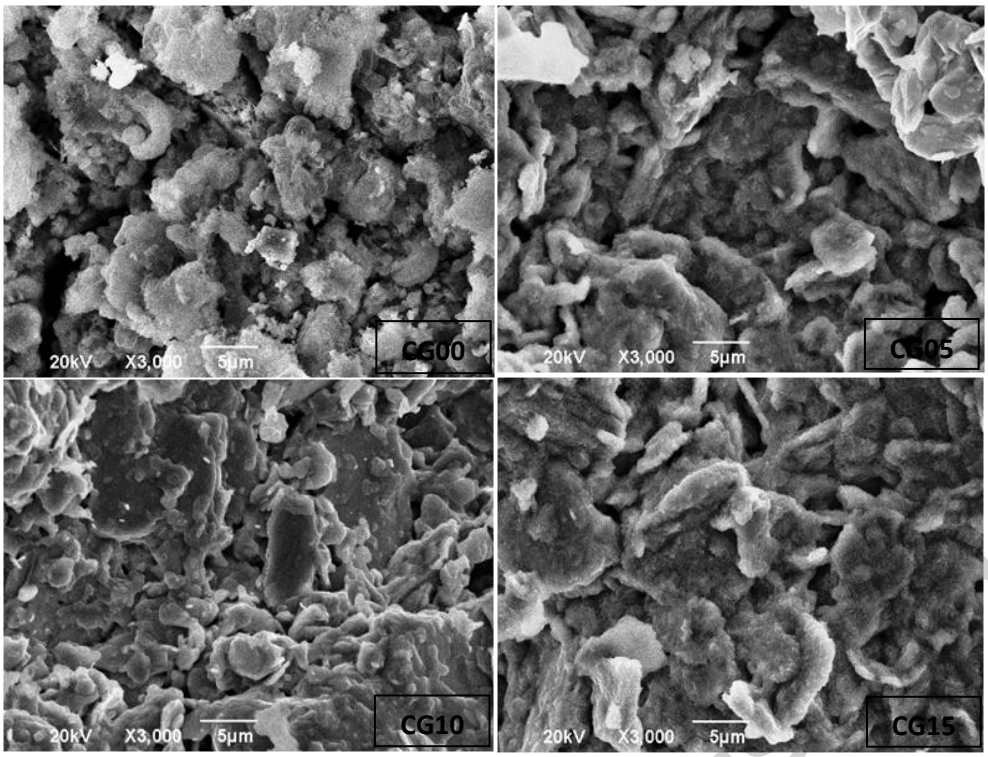

Fig. 3. SEM micrographs of resistivity for $Bi_{1.6}Pb_{0.4}Sr_2Ca_{1-x}Gd_xCu_2O_{8+\delta}$ samples.

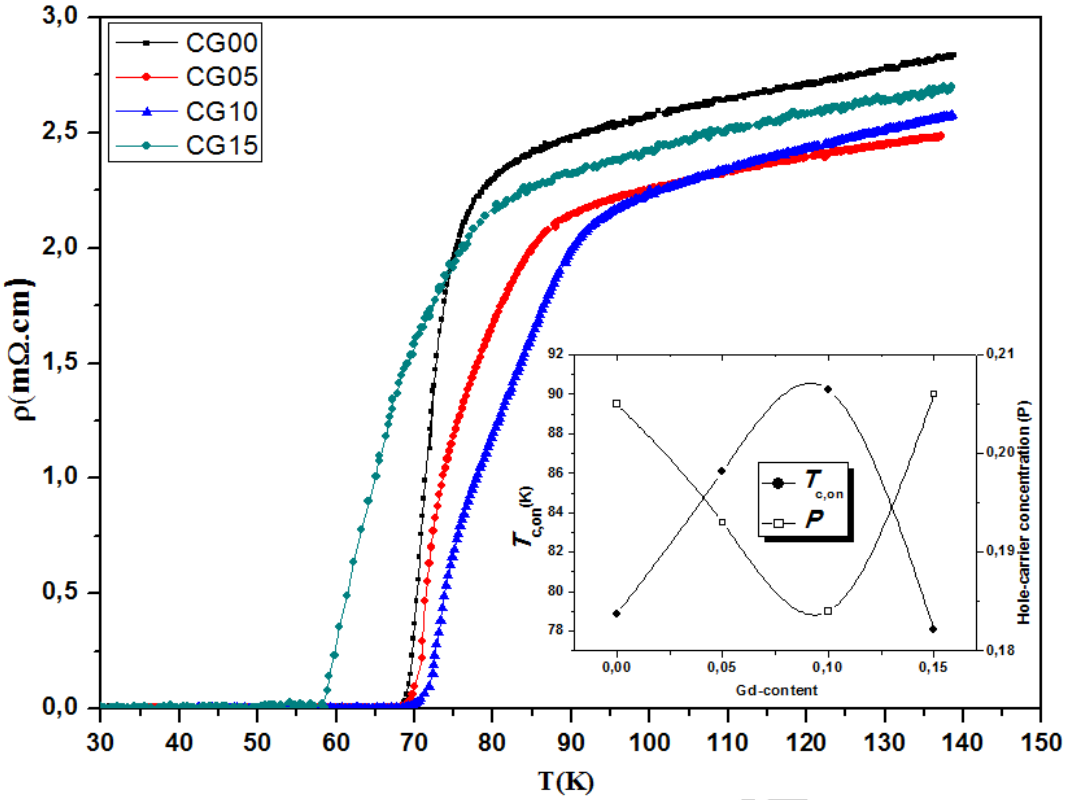

Fig. 4. Temperature dependence of resistivity for $Bi_{1.6}Pb_{0.4}Sr_2Ca_{1-x}Gd_xCu_2O_{8+\delta}$ samples. Insets: $T_{c,on}$ and Hole-carrier concentration vs Gadolinium content.

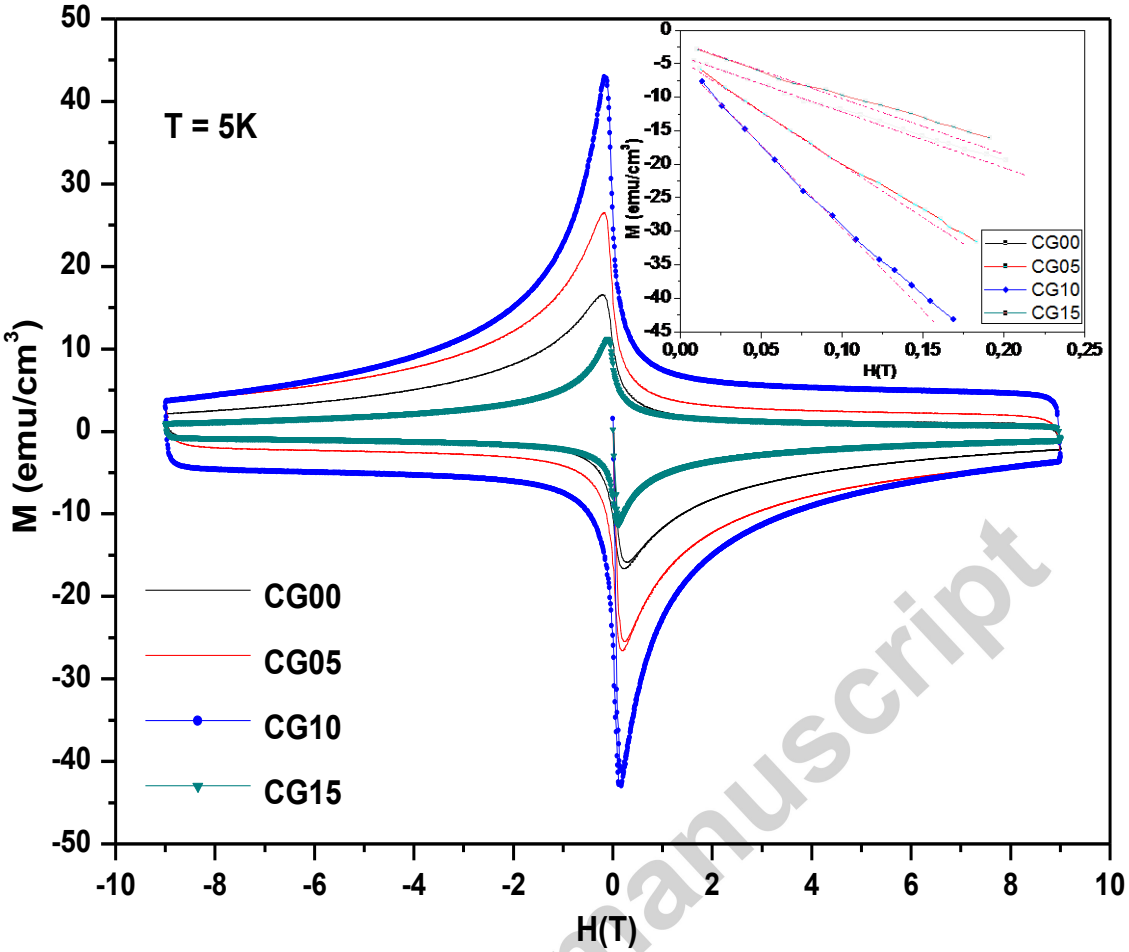

Fig. 5. Magnetic hysteresis loops measured at 5 K for $Bi_{1.6}Pb_{0.4}Sr_2Ca_{1-x}Gd_xCu_2O_{8+\delta}$ samples. The inset displays the field dependence of initial magnetization curves.

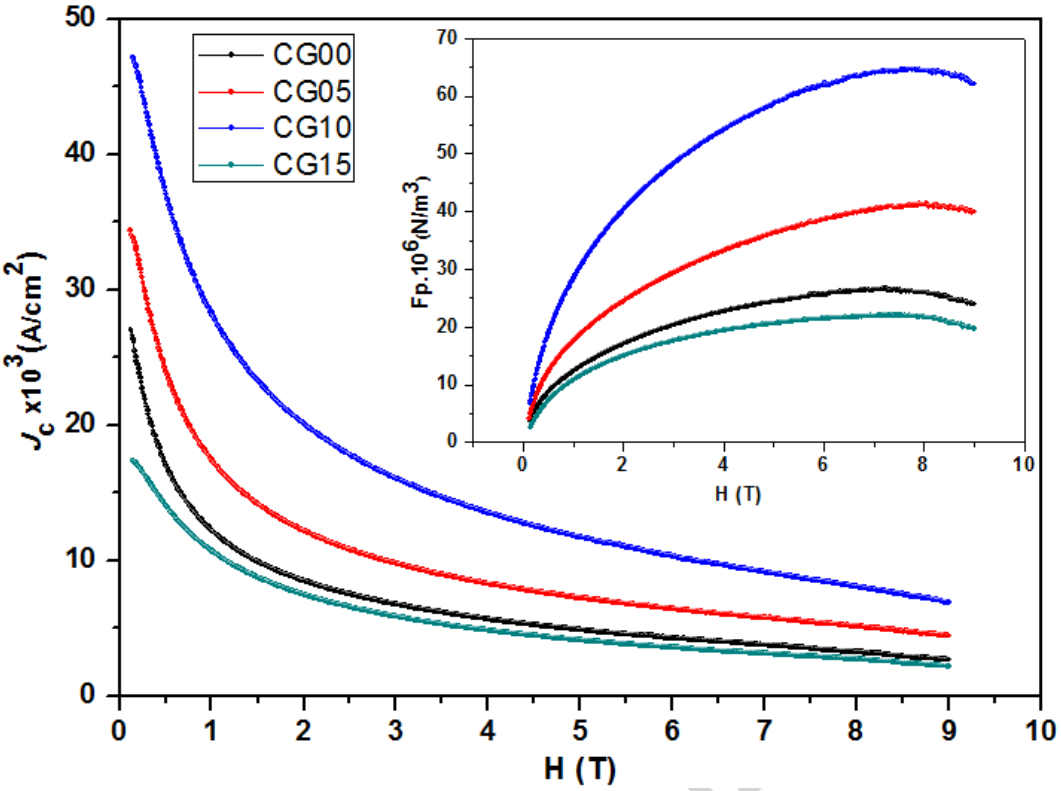

Fig. 6. Critical current densities of $Bi_{1.6}Pb_{0.4}Sr_2Ca_{1-x}Gd_xCu_2O_{8+\delta}$ samples at 5K as a function of applied field. Inset: variation of pinning force versus magnetic field.